Eletrônica de Potência
Open Journal of Power Electronics

Received July 31, 2024; accepted October 02, 2024; Date of publication October 14, 2024.
The review of this paper was arranged by Associate Editor Fernanda M. Carnielutti and Editor-in-Chief Heverton A. Pereira.

Digital Object Identifier http://doi.org/10.18618/REP.e202440

Adaptive Frequency-Based Power Management for Off-Grid Hybrid Photovoltaic Converters

Ezequiel Gonschorowski[1], Rafael Cardoso[1], Edivan Laercio Carvalho[2], Carlos Marcelo de Oliveira Stein[1], Emerson Giovani Carati[1], Gustavo Weber Denardin[1], Jean Patric da Costa[1]

[1]Federal University of Technology - Paraná - UTFPR, Pato Branco - PR, Brazil.
[2]Tallinn University of Technology - Tallinn - Estonia.

e-mail: gonschorowski@alunos.utfpr.edu.br, rcardoso@utfpr.edu.br, edivan.carvalho@taltech.ee, cmstein@utfpr.edu.br, emerson@utfpr.edu.br, gustavo@utfpr.edu.br, jeanpatric@utfpr.edu.br.

ABSTRACT The intermittency in photovoltaic systems (PV) can lead to power quality issues, especially in off-grid applications. In these cases, adding an energy storage element helps to cope with the intermittency to provide adequate power to the local load. In this scenario, combining Li-Ion batteries and supercapacitors as a hybrid energy storage system (HESS) is powerful due to the battery's high energy density and the supercapacitor's high power density. The HESS demands adequate power management to operate adequately. This paper proposes an adaptive frequency-based power management for a Li-Ion battery and supercapacitor HESS applied to an off-grid PV converter. The main idea of this strategy is to guarantee a smoother current in the battery and reduce the power dissipation in the HESS. The smoother battery current transition helps avoid excessive battery stress and improves lifespan. The proposed strategy is compared with two other strategies. The results show that the proposed approach is more efficient in reducing the HESS' power dissipation and providing smooth current variations to the battery.

KEYWORDS Power Management, Hybrid Energy Storage Systems, Li-Ion Battery, Supercapacitor, Off-Grid Hybrid Photovoltaic Converters, Photovoltaic Systems.

I. INTRODUCTION

The increase in greenhouse gases, environmental concerns, and the future depletion of fossil fuels drive the search for renewable energy resources. Among renewable options, photovoltaic (PV) systems have gained attention in residential areas due to their economic viability across various scales and applications, including low power levels uses [1]. Given this backdrop, PV inverters combined with storage elements have garnered attention in recent industrial developments for their flexibility in adding energy storage to compensate for intermittent generation [2].

Combining two or more storage elements, such as batteries, fuel cells, supercapacitors, and others, results in the so-called hybrid energy storage system (HESS). In [3], various storage element technologies and their use are compared. Among them, pairing a supercapacitor and battery is an interesting combination because the supercapacitor complements the low power density of the battery. In contrast, the battery addresses the low energy density of the supercapacitor. This combination helps to mitigate fluctuations in power generation from the PV system. However, it requires a complex power electronics interface, which is a disadvantage [4] and the battery bank must be correctly selected for supply the demand of the system [5].

The topologies for HESS with a battery and a supercapacitor can be categorized as passive, semi-active, and fully active. The passive topology is the simplest and most cost-effective. In this configuration, the battery and supercapacitor are directly connected to the dc bus, making it challenging to match the bus voltage level, mainly because high-voltage supercapacitors and batteries are expensive. Since the battery and supercapacitor share the same terminal voltage, the HESS dynamics are primarily dictated by the battery's state of charge (SOC) [6].

The semi-active topology is similar to the passive one but incorporates a converter between one storage element and the dc bus. This topology allows for control over the power flow of one energy storage element. However, the storage element directly coupled to the dc bus will still require voltage specifications compatible with the dc bus [7].

The fully active topology addresses the problem of the need to use high-voltage storage elements. This configuration involves placing a bidirectional converter between each energy storage element and the dc bus. It allows storage elements with a different voltage than the dc bus and increases flexibility due to improved power flow control [8]. On the other hand, the fully active topology should be associated with appropriate power management to achieve adequate energy usage.

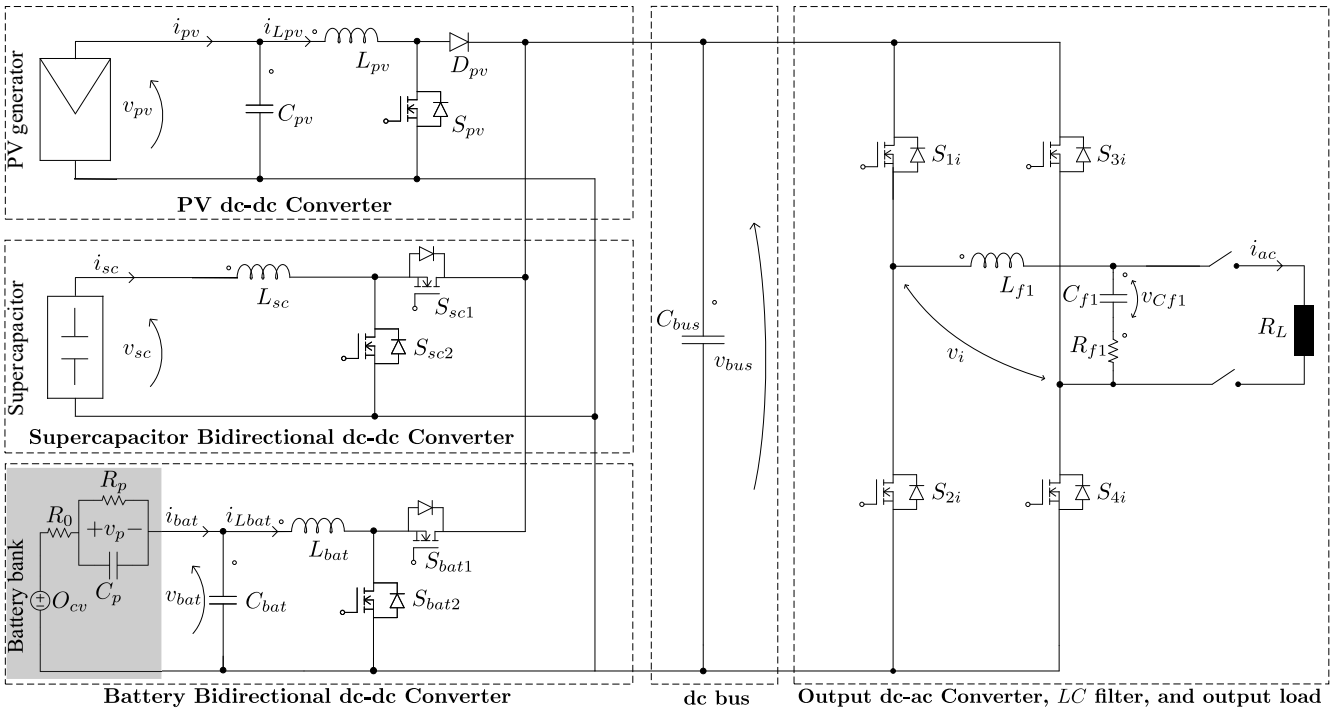

FIGURE 1. Hybrid photovoltaic inverter with supercapacitor and Li-Ion battery.

There are various ways to implement a HESS power management system. In [9], the authors present several system management strategies. The rule-based approach is well used due to its simple implementation and involves implementing rules through look-up tables or conditional statements [10]. This approach, being the most straightforward, demands the least computational effort among the presented strategies. However, its real-time optimization and adaptability are challenging [11], [12]. Furthermore, due to the lack of a modeling system, the rule-based management does not work very well to answer the system's dynamic response [13].

Frequency-based power management is another possibility. This approach decomposes the power signal into high and low-frequency components. Since the supercapacitor provides a fast transient response, the high-frequency power component is associated with the supercapacitor, while the low-frequency power component is related to the battery [14]. In [15], it is demonstrated the frequency-based method reduces the magnitude of root means square (RMS) and the maximum peak of the battery's current. In [16], the authors demonstrate the reduction in RMS current implies a reduction of the power dissipation in the HESS composed of battery and supercapacitor.

Other very effective strategies rely on optimization. However, they are mathematically and computationally demanding [2], [17]. Other strategies used for managing systems using batteries are based on artificial intelligence. Although efficient, artificial intelligence approaches demand significant data for training and validation of the algorithm that leads to extensive tests [18], [19], [20].

The authors in [21] describe HESS as a solution for various applications in renewable energy, such as emergency systems, electric vehicles, backup systems, telecommunication, public lighting, data centers, hospitals, and commercial buildings.

Integrating energy storage elements with photovoltaic generation can provide continuous power, essential in remote locations or critical areas where power interruptions occur. Integrating HESS with a photovoltaic inverter leads to different operation scenarios that can be explored depending on whether grid-tie or off-grid mode is considered [22]. Especially in off-grid operations, only using a battery to regulate or keep the power flow to the load can significantly reduce the battery lifespan. Therefore, using a HESS with an adequate power management strategy can reduce the use of the battery during the operation and, consequently, increase its life cycle.

This paper considers a hybrid inverter for off-grid operation using supercapacitors and lithium-ion (Li-Ion) batteries. A simple and effective adaptive frequency-based strategy of power management is proposed. The proposed power management modifies the cutoff frequency of a filter used in the power management algorithm based on the batteries' State of Power (SOP) and State of Energy (SOE). It provides smoother battery currents, reducing high-frequency components that can degrade the battery's lifespan. The proposed strategy is compared with the rule-based method and the traditional frequency-based method, which are two other methods of simple implementation.

Since SOC estimation is used in any Li-Ion battery application demanding correct operation of the battery, the implementation of the proposed strategy is straightforward. This is due to the fact the proposed approach relies on information already available during the SOC estimation process and other information easily found in datasheets. It avoids complex algorithms with extensive calculations, such as those using optimization methods or laborious data set creation and training involved in artificial intelligence approaches.

This work is an extension of [23]. This extended paper introduces a new adaptive frequency-based power management strategy and compares the results using the approaches proposed in [24] and [25].

II. SYSTEM DESCRIPTION

Fig. 1 illustrates the hybrid photovoltaic converter under study. The system encompasses four converters: a boost converter [26], two classic buck/boost bidirectional converters [27], [28] and an inverter [29]. The boost converter is responsible for extracting the energy from the photovoltaic panels, and it uses two algorithms to assist in managing the energy system. The first is a Maximum Power Point Tracking (MPPT) algorithm, responsible for extracting the maximum power available in the PV panels. The second is a Limited Power Point Tracking (LPPT) algorithm that limits the PV panels' extracted power. The MPPT and LPPT are explained in [30], [31].

The buck/boost bidirectional converters charge or discharge the battery and the supercapacitor. The buck/boost bidirectional converter connected to the battery controls the dc bus voltage through the charging/discharging process. An equivalent first-order RC model represents the battery bank [32]. The inverter delivers power from the dc bus to the ac load. With these four converters, the system's management can process the desired power, charge/discharge the battery, charge/discharge the supercapacitor, limit the extracted power from PV panels, or extract the maximum power and power the load.

All the transfer functions and the control loops for the correct operation of the hybrid inverter described in Fig. 1 are presented in [23]. A Kalman Filter estimates the battery State of Charge (SOC_{BAT}) as described in [32]. The supercapacitor State of Charge (SOC_{SC}) is obtained using:

$$SOC_{SC} = \frac{v_{sc}}{v_{sc_{max}}}, \tag{1}$$

where, v_{sc} is the instantaneous supercapacitor voltage and $v_{sc_{max}}$ is the maximum rated voltage of the supercapacitor.

III. POWER MANAGEMENT OF THE SYSTEM

This section discusses the proposed power management strategy and two other approaches used for comparison. All strategies use the storage elements when the power generated by the PV array either falls short of or exceeds the load's power. The system channels the surplus PV energy into the storage elements or discharges them to power the load. Subsections A and B summarize the rule-based [24] and frequency-based [25] algorithms, respectively, used for comparison purposes, while subsection C presents the proposal.

A. Rule-based power management

The main idea of this power management is to use the supercapacitor until it reaches the maximum or minimum SOC. After that, the management uses the battery to supply the power demand. Algorithm 1 presents the implementation of the rule-based management approach.

The power demand (P_{DM}) is the difference between the power of the load (P_L) and the generated power by the PV array (P_{PV}):

$$P_{DM} = P_L - P_{PV}. \tag{2}$$

Since the converter associated with the battery regulates the dc bus voltage, the reference of power for charging and discharging the supercapacitor is:

$$P^*_{SC} = P_{DM}. \tag{3}$$

Algorithm 1 Rule-based power management

$P_{DM} = P_L - P_{PV}$
if $P_{DM} \leq 0$ **then**
  if $SOC_{SC} \leq 0.95$ **then**
    $MPPT \rightarrow ON$
    $Supercapacitor \rightarrow Charging\ with\ P^*_{SC} = P_{DM}$
  else if $SOC_{BAT} \leq 0.95$ **then**
    $MPPT \rightarrow ON$
    $Supercapacitor \rightarrow OFF$
    $Battery \rightarrow Charging$
  else if $SOC_{BAT} > 0.95$ **then**
    $LPPT \rightarrow ON$
    $Supercapacitor \rightarrow OFF$
  end if
else
  if $SOC_{SC} \geq 0.5$ **then**
    $MPPT \rightarrow ON$
    $Supercapacitor \rightarrow Discharging\ with\ P^*_{SC} = P_{DM}$
  else if $SOC_{BAT} \geq 0.2$ **then**
    $MPPT \rightarrow ON$
    $Supercapacitor \rightarrow OFF$
    $Battery \rightarrow Discharging$
  else if $SOC_{BAT} < 0.2$ **then**
    $Disconnect\ the\ load$
  end if
end if

In this power management strategy, when the power generation is equal to or exceeds the power of the load ($P_{DM} \leq 0$), the SOC_{SC} is verified. Until the SOC_{SC} reaches 95%, the MPPT is active, and the supercapacitor

is charged with a power reference given by (3). The power flow to the battery is only responsible for regulating the dc bus voltage. When the supercapacitor is charged ($SOC_{SC} > 95\%$), and the battery is not charged ($SOC_{BAT} \leq 95\%$), the power manager activates the MPPT, turns off the supercapacitor and the battery charges assuming the excessive generated power balancing the dc bus. When the battery is charged ($SOC_{BAT} > 95\%$), the LPPT is active, limiting the generated power, and the supercapacitor is disabled.

When the power generation lacks the power of the load ($P_{DM} > 0$), while the SOC_{SC} is greater or equal to 50%, the MPPT is active, and the supercapacitor provides power to the load with a power reference given by (3). The power flow to the battery is only responsible for regulating the dc bus voltage. When the supercapacitor is depleted ($SOC_{SC} < 50\%$) and the battery still has stored energy ($SOC_{BAT} \geq 20\%$), the power manager activates the MPPT, turns off the supercapacitor and the battery provides additional power to the load balancing the dc bus. When the battery is depleted ($SOC_{BAT} < 20\%$), there is no available power from the PV array and energy storage elements. Therefore, the power manager disconnects the load.

B. Frequency-based power management with fixed cutoff frequency

The main idea of this power management is to decompose the power demand (P_{DM}) into low and high-frequency components. The battery assumes the low-frequency component due to its low power density. The supercapacitor assumes the high-frequency component due to its high power density [16].

The structure presented in Fig. 2 generates the power references for the battery (P^*_{BAT}) and supercapacitor (P^*_{SC}). The LPF block is a first-order low-pass filter with a cutoff frequency given by [25]:

$$f_c[Hz] = \frac{\rho_{power}}{3600\rho_{energy}}, \tag{4}$$

where, ρ_{power} is the power density of the battery in W/kg and ρ_{energy} is the energy density of the battery in Wh/kg.

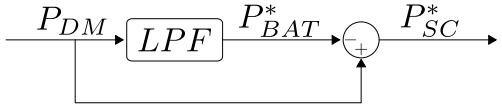

FIGURE 2. Block diagram of the frequency-based power management.

The reference for the battery power (P^*_{BAT}) is obtained using:

$$\begin{aligned} P_{BAT}[k] &= (1-\alpha)P_{BAT}[k-1] + \alpha P_{DM}[k], \\ \alpha &= \frac{T_s}{T_s + \frac{1}{2\pi f_c}}, \end{aligned} \tag{5}$$

where, T_s is the sampling period of the power manager and f_c is the cutoff frequency given by (4).

The implementation of this management strategy follows the algorithm 2 described in the following subsection. The only difference is the fixed cutoff frequency used in this method.

C. Adaptive frequency-based power management

Since the system is dynamic, maintaining a fixed cutoff frequency can interfere with the correct power distribution in the HESS, especially with variable loads that can lead to battery degradation [16]. The intermittent generation profile of the photovoltaic generation also worsens this phenomenon. Therefore, this subsection proposes an adaptive frequency-based power management strategy for the hybrid inverter.

The proposed management strategy uses adaptation to modify the cutoff frequency f_c in real-time in equation (5). The cutoff frequency of the filter is calculated using:

$$f_c[Hz] = \frac{SOP}{SOE}, \tag{6}$$

where, SOP is the State of Power, and SOE is the State of Energy of the battery. The SOP estimates how much power the battery can deliver at a given moment, and the SOE is the available energy in the battery at that instant [33].

The SOE estimation is shown in [34], and it is related to the SOC_{BAT} by:

$$SOE = 3600 v_{bat} Q_{max} SOC \ [Ws], \tag{7}$$

where, Q_{max} is the actual battery's maximum capacity, measured in Ah.

The authors of [35] present the State of Power (SOP) estimation. Given that a positive battery current represents the discharging process, when the battery is discharging, the $SOP_{discharge}$ is given by:

$$\begin{aligned} SOP_{discharge} = \min\{&SOP^V_{discharge},\ SOP^I_{discharge},\\ &SOP^{SOC_{BAT}}_{discharge}\}, \end{aligned} \tag{8}$$

where,

$$\begin{cases} SOP^V_{discharge} = V_{min}\frac{(O_{cv} - v_p - V_{min})}{R_p}, \\ SOP^I_{discharge} = (O_{cv} - v_p - R_0 I_{max}) I_{max}, \\ SOP^{SOC_{BAT}}_{discharge} = \frac{3600 Q_{max}(SOC_{BAT} - SOC_{BAT_{min}}) v_{bat}}{T}. \end{cases} \tag{9}$$

When the battery is charging, the SOP_{charge} is determined by:

$$SOP_{charge} = \max\{SOP^V_{charge},\ SOP^I_{charge},\ SOP^{SOC_{BAT}}_{charge}\}, \tag{10}$$

where,

$$\begin{cases} SOP^V_{charge} = V_{max}\frac{(O_{cv} - v_p - V_{max})}{R_p}, \\ SOP^I_{charge} = (O_{cv} - v_p - R_0 I_{min}) I_{min}, \\ SOP^{SOC_{BAT}}_{charge} = \frac{3600 Q_{max}(SOC_{BAT} - SOC_{BAT_{max}}) v_{bat}}{T}. \end{cases} \tag{11}$$

For a discharge process, the $SOP^V_{discharge}$ indicates the battery's power associated with a voltage applied to the

battery equal to the minimum operating voltage (V_{min}) specified by the manufacturer. The $SOP^{I}_{discharge}$ indicates the battery's power associated with the maximum discharging current ($I_{max} > 0$) determined by the manufacturer. The $SOP^{SOC_{BAT}}_{discharge}$ indicates the battery's power necessary to achieve a desired minimum State of Charge ($SOC_{BAT_{min}}$) in the time interval $T[s]$.

Similarly, for a charging process, the SOP^{V}_{charge} indicates the battery's power associated with a voltage applied to the battery equal to the maximum operating voltage (V_{max}) specified by the manufacturer. The SOP^{I}_{charge} indicates the battery's power associated with the minimum discharging current ($I_{min} < 0$) determined by the manufacturer. The $SOP^{SOC_{BAT}}_{charge}$ indicates the battery's power necessary to achieve a desired maximum State of Charge ($SOC_{BAT_{max}}$) in the time interval $T[s]$.

The O_{cv} is the Open Circuit Voltage of the battery, v_p is the voltage drop in the RC parallel pair of the equivalent circuit model of the battery shown in Fig. 1. The element R_p is the resistor in parallel with the C_p capacitor, while R_0 is the series resistor of the equivalent circuit of the battery.

Algorithm 2 shows the proposed management strategy. The converter associated with the battery is always responsible for regulating the dc bus.

When the power generation is equal to or exceeds the power of the load ($P_{DM} \leq 0$), the cutoff frequency of the low-pass filter is updated considering the SOP_{charge}. There are four situations to be considered.

If both the battery and supercapacitor are not charged (SOC_{BAT} and $SOC_{SC} \leq 95\%$), the MPPT is active, and the battery and supercapacitor are charging with power references for the battery and supercapacitor given by $P^{*}_{BAT}[k]$ and $P^{*}_{SC}[k]$, respectively.

When the battery is not charged ($SOC_{BAT} \leq 95\%$) but the supercapacitor is charged ($SOC_{SC} > 95\%$), the supercapacitor is turned off and the LPPT is activated. The LPPT is used to provide a smooth current profile to charge the battery that is proportional to the power reference given by $P^{*}_{BAT}[k]$ while the power reference for the LPPT is $P^{*}_{PV}[k]$.

When the battery is charged ($SOC_{BAT} > 95\%$) but the supercapacitor is capable of storing additional energy ($SOC_{SC} \leq 95\%$), the MPPT is active because of the high power density of the supercapacitor and only this element is charging with power reference defined by P^{*}_{SC}.

In the case both the battery and supercapacitor are charged (SOC_{BAT} and $SOC_{SC} > 95\%$), the power manager activates the LPPT, the supercapacitor is turned off, and the converter associated with the battery keeps providing power balance to the dc bus.

When the power generation is lower than the power load ($P_{DM} > 0$), the storage elements need to supply the power deficit. The power manager activates the MPPT to extract all possible power from the PV array. If both the battery and the supercapacitor have enough energy to supply the load ($SOC_{BAT} \geq 20\%$ and $SOC_{SC} \geq 50\%$), the cutoff frequency of the low-pass filter is updated considering the $SOP_{discharge}$ and the battery and supercapacitor provide power to the load according to the references $P^{*}_{BAT}[k]$ and $P^{*}_{SC}[k]$, respectively.

When the supercapacitor is depleted ($SOC_{SC} < 50\%$) but the battery still can provide power to the load ($SOC_{BAT} \geq 20\%$), the battery is the only storage element responsible for supplying the deficit of power. Since the converter associated with the battery is responsible for balancing the dc bus, it is made automatically.

In the case the battery is depleted ($SOC_{BAT} < 20\%$) but the supercapacitor is capable of supplying power ($SOC_{SC} \geq 50\%$), the supercapacitor provides power to the load with a power reference given by $P^{*}_{SC} = P_{DM}$.

Algorithm 2 Adaptive frequency-based power management

$P_{DM} = P_L - P_{PV}$
if $P_{DM} \leq 0$ **then**
  $f_c = SOP_{charge}/SOE$
  $\alpha = T_s/(T_s + \frac{1}{2\pi f_c})$
  if $SOC_{BAT} \leq 0.95$ & $SOC_{SC} \leq 0.95$ **then**
    $MPPT \rightarrow ON$
    $P^{*}_{BAT}[k] = (1-\alpha)P^{*}_{BAT}[k-1] + \alpha P_{DM}[k]$
    $P^{*}_{SC}[k] = P_{DM}[k] - P^{*}_{BAT}[k]$
  else if $SOC_{BAT} \leq 0.95$ & $SOC_{SC} > 0.95$ **then**
    $Supercapacitor \rightarrow OFF$
    $LPPT \rightarrow ON$
    $P^{*}_{BAT}[k] = (1-\alpha)P^{*}_{BAT}[k-1] + \alpha P_{DM}[k]$
    $P^{*}_{PV}[k] = P_L + P^{*}_{BAT}[k]$
  else if $SOC_{BAT} > 0.95$ & $SOC_{SC} \leq 0.95$ **then**
    $MPPT \rightarrow ON$
    $Supercapacitor \rightarrow charging$ with $P^{*}_{SC} = P_{DM}$
  else if $SOC_{BAT} > 0.95$ & $SOC_{SC} > 0.95$ **then**
    $LPPT \rightarrow ON$
    $Supercapacitor \rightarrow OFF$
  end if
else
  $MPPT \rightarrow ON$
  if $SOC_{BAT} \geq 0.2$ & $SOC_{SC} \geq 0.5$ **then**
    $f_c = SOP_{discharge}/SOE$
    $\alpha = T_s/(T_s + \frac{1}{2\pi f_c})$
    $P^{*}_{BAT}[k] = (1-\alpha)P^{*}_{BAT}[k-1] + \alpha P_{DM}[k]$
    $P^{*}_{SC}[k] = P_{DM}[k] - P^{*}_{BAT}[k]$
  else if $SOC_{BAT} \geq 0.2$ & $SOC_{SC} < 0.5$ **then**
    $Supercapacitor \rightarrow Off$
  else if $SOC_{BAT} < 0.2$ & $SOC_{SC} \geq 0.5$ **then**
    $Supercapacitor \rightarrow discharging$ with $P^{*}_{SC} = P_{DM}$
  else if $SOC_{BAT} < 0.2$ & $SOC_{SC} < 0.5$ **then**
    $Disconnect\ the\ load$
  end if
end if

Finally, when both the battery and supercapacitor are depleted ($SOC_{BAT} < 20\%$ and $SOC_{SC} < 50\%$), there is not enough power to supply the load, and the power manager disconnects the load.

IV. REAL-TIME HARDWARE-IN-THE LOOP RESULTS

This section presents the real-time hardware-in-the-loop results obtained. Experiments were conducted using a Typhoon HIL 602+ platform to evaluate the algorithms introduced in the preceding section. The TMS320F28379D microcontroller was used to implement the controllers and power management systems. A real irradiance profile sampled each 1 second was used for the tests, as illustrated in Fig. 3. A variable load profile was also used to test the efficiency of the implemented power management strategies.

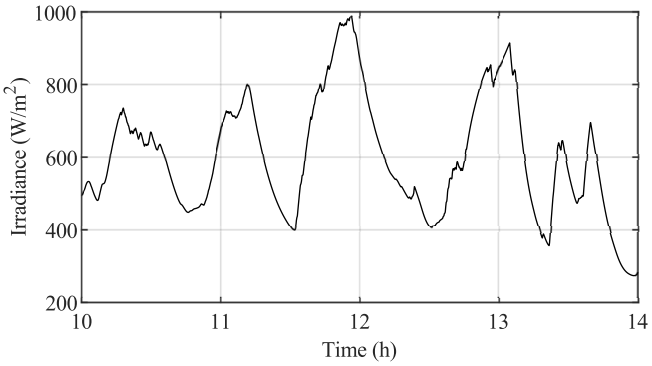

FIGURE 3. Irradiance profile.

The photovoltaic array consists of four Canadian Solar KuMax CS3U-355P [36] panels connected in series. Each panel delivers a peak power of 355 W_p and has an open-circuit voltage of 46.8 V, resulting in a combined total power of 1420 W_p and 187.2 V.

To ensure an adequate voltage for the converter gain, ten XTM-18R0626-R supercapacitor [37] units connected in series are used. This arrangement provides 3.4 Wh of energy and a maximum voltage of 180 V.

The battery has a nominal voltage of 96 V and a capacity of 20 Ah. The battery bank is composed of ICR18650-22f cells [38]. The battery's maximum power density is 356.18 W/kg, and its maximum energy density is 173.82 Wh/kg. Therefore, the cutoff frequency for the frequency-based method presented in subsection B is 0.00057 Hz.

The dc bus voltage is 380 V. All converters operate with a 50 kHz switching frequency. Table 1 presents the converters' parameters and specifications. The power manager frequency operation is 1 Hz. The control system structure details can be found in [23].

Fig. 4 shows the system operation using the proposed power management strategy. In Fig. 4(a), the PV generated power is greater or equal to the load ($P_{DM} \leq 0$). The initial conditions of the storage elements are $SOC_{BAT} = 0.9453$ and $SOC_{SC} = 0.526$. In Region 1, both storage elements are charging, and the region is associated with line 5 of the algorithm 2. In Region 2, the supercapacitor is charged, and the battery keeps charging with $LPPT$ activated to avoid abrupt power changes in the battery, according to line 9 of the algorithm 2. Region 3 is associated with line 17. In this region, the $LPPT$ is active because both storage elements are fully charged, and the algorithm extracts the power needed to supply the load and keep the dc bus balance.

TABLE 1. Converters' Parameters and Specifications.

PV dc-dc Converter	
Parameter	**Specification**
L_{pv}	1.3 mH
C_{pv}	2.3 μF
Supercapacitor Bidirectional dc-dc Converter	
Parameter	**Specification**
L_{SC}	2.4 mH
Battery Bidirectional dc-dc Converter	
Parameter	**Specification**
L_{bat}	2.4 mH
C_{bat}	1.3 μF
Output dc-ac Converter	
Parameter	**Specification**
L_{f1}	125μH
C_{f1}	5 μF
R_{f1}	1.5 Ω
C_{bus}	1200 μF

In Fig. 4(b), the PV generated power is insufficient to supply the load ($P_{DM} > 0$). The initial conditions of the storage elements are $SOC_{BAT} = 0.222$ and $SOC_{SC} = 0.885$. Region 4 relates with line 23 of the algorithm 2. In this region, both storage elements are discharging to supply the power deficit to the load. Region 5 refers to line 28, where the supercapacitor is fully discharged. Therefore, the manager turns the supercapitor off. Due to its intrinsic dc bus regulation characteristic, the battery complements the power needed to supply the load. Region 6 depicts when both storage elements lack the minimum energy to supply the load. Hence, the load is disconnected, and the battery can use P_{PV} for charging.

Fig. 5 presents the operation results of the power management algorithms including the PV generated power (P_{PV}), load (P_L), power of the supercapacitor (P_{SC}), and the battery's output power (P_{BAT}) in the left axes, and in the right axes the State of Charge (SOC) of battery and supercapacitor. In this figure, a positive power value indicates that the HESS is discharging, while a negative value signifies charging.

Fig. 5(a) depicts the results for the rule-based management. Fig. 5(b) shows the results of frequency-based management with fixed low-pass filter cutoff frequency. The results of the proposed adaptive power manager are shown in 5(c).

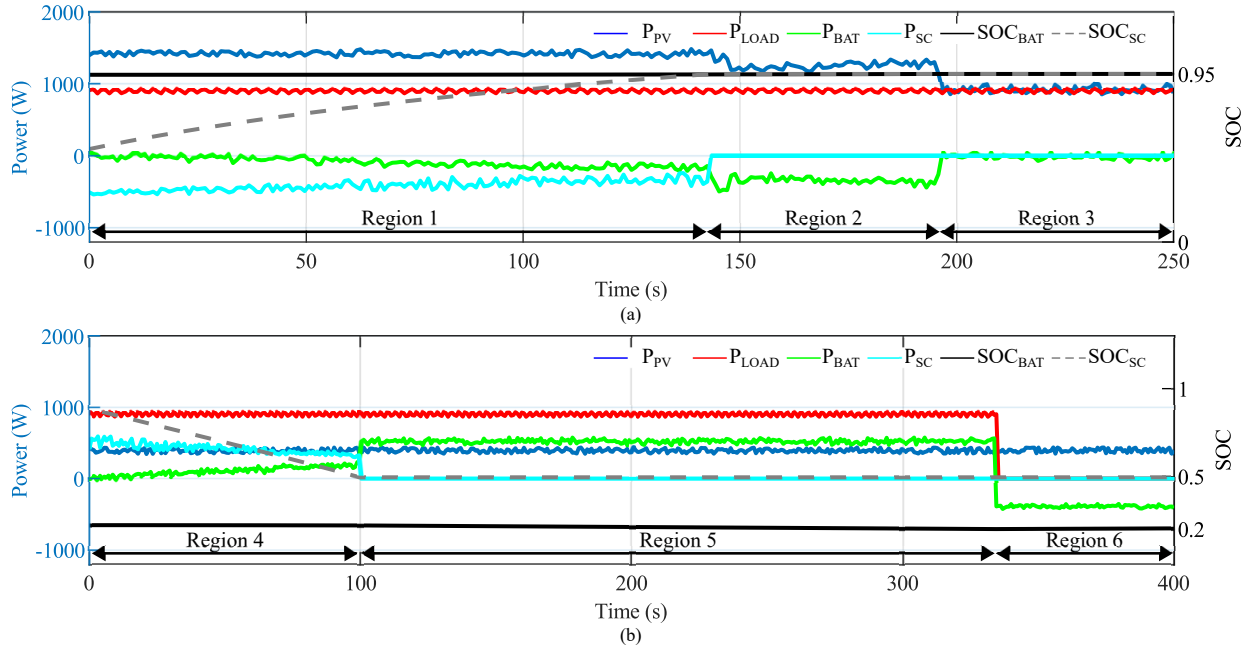

FIGURE 4. System operation using the proposed power management strategy: (a)$P_{DM} \leq 0$, (b)$P_{DM} > 0$.

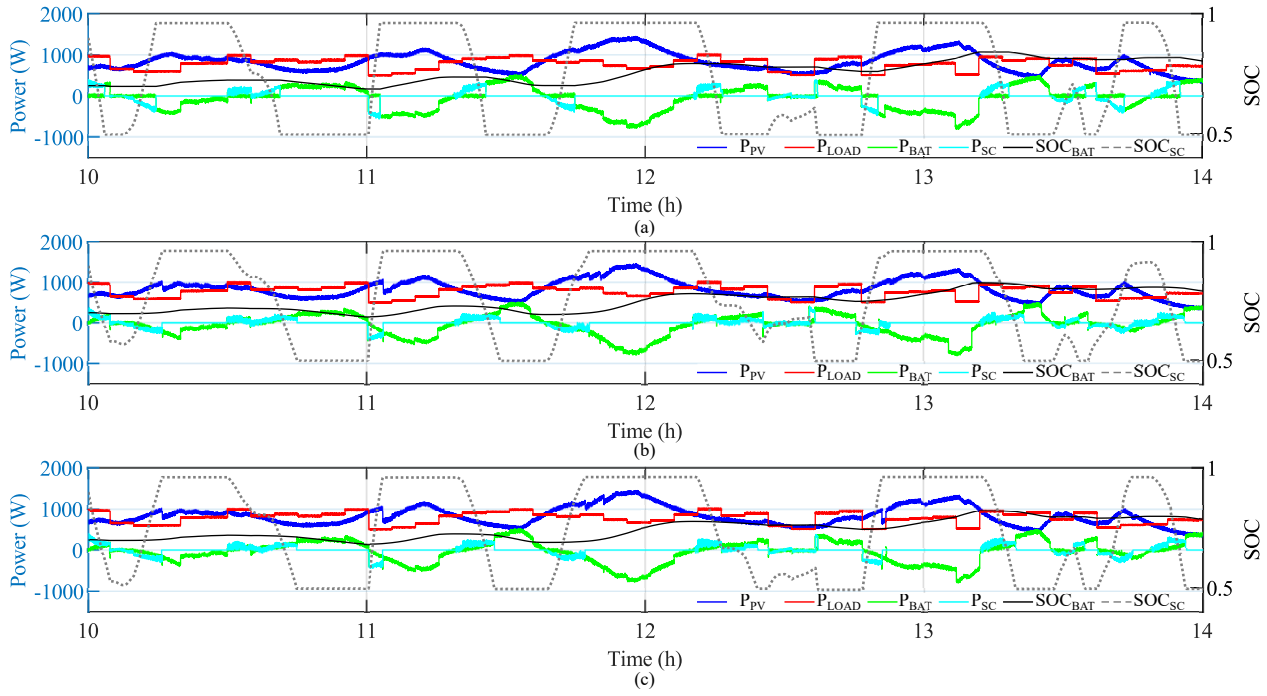

FIGURE 5. Real-time results for the different power management strategies: (a) rule-based management; (b) Fixed cutoff frequency; (c) Proposed method.

To explain the behavior of the power management methods, the gray area in Fig. 5 is considered. When there is a surplus of generation ($P_{DM} < 0$), the HESS can be charged. In Fig. 5(a), using the rule-based method, the supercapacitor is first charged, and the battery assumes the exceeding power after the supercapacitor charge. There is an abrupt change in battery current when this strategy is used. With the frequency-based management strategies presented in Fig. 5(b) and 5(c), the battery assists the supercapacitor in handling this power surplus. It begins to charge with the supercapacitor while respecting the filtered power reference. Unlike rule-based management, the battery does not experience a current step when the supercapacitor is fully charged.

Those current step variations impact the battery's lifespan and provide higher power dissipation. Power dissipation increases the battery's temperature, and if the temperature is not adequately controlled, the battery life is reduced [39]. To compare the energy loss dissipated in the battery using the three power management methods, the battery's equivalent series resistance (ESR) is considered. The ESR of the battery is $R_0 = 0.2172\ \Omega$. During the experiment, the proposed strategy dissipated less power in the battery than rule-based management; the proposed approach has 12.48% less power dissipation. Compared to the fixed cutoff frequency, the proposed strategy has 5.3% less power dissipated in the battery.

Another metric for comparison is the overall energy loss in the HESS. It considers the power dissipated in the battery and supercapacitor. The energy dissipation in the supercapacitor is calculated using its ESR of 0.22Ω. Compared to the rule-based management system, the proposed strategy provides 5.55% less dissipation. The proposed method offers 1.76% less power dissipation than the fixed cutoff frequency-based strategy. Therefore, the proposed approach has better energy efficiency.

The current variation of the battery can be quantified using the root mean square value of the battery current calculated over the whole time windows of the experiment. The RMS current for the rule-based method is 2.7575 A. The fixed frequency-based method gives 2.6542 A, and the proposed strategy gives 2.5798 A. This reduction provided by the proposed approach reduces the battery's stress and corroborates the method's contribution to the battery's lifespan.

Fig. 6 depicts the SOC_{BAT} profile obtained using the three power management methods. The battery cycle usage for the rule-based method is 16.44% while the fixed cutoff frequency-based method provides 17.25%. The proposed power management method gives 16.57% of battery usage. Since the rule-based method prioritizes the supercapacitor charge/discharge over the battery, it uses fewer battery cycles than the fixed cutoff frequency-based method that uses both battery and supercapacitor during the charge/discharge process. The proposed adaptive frequency-based method provides battery usage similar to the rule-based method.

Fig. 7 shows the behavior of the cutoff frequency calculated by the proposed management strategy. In Fig. 7, it is possible to see that the proposed management system does reach the cutoff frequency value of $0.00057\ Hz$ used in the fixed cutoff frequency-based method. With a low-pass filter with a lower bandpass, the change in the power reference for the battery is smoother than the previous method, as shown by the results.

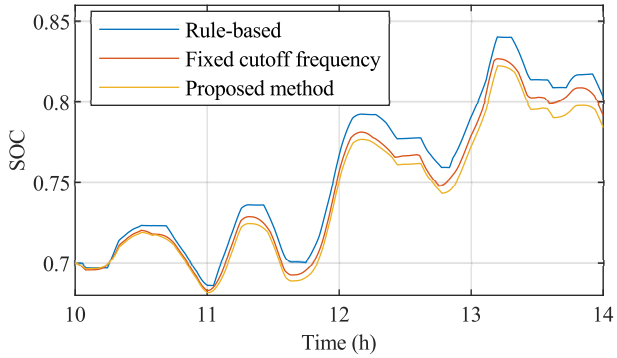

FIGURE 6. Battery state of charge for the three tested strategies.

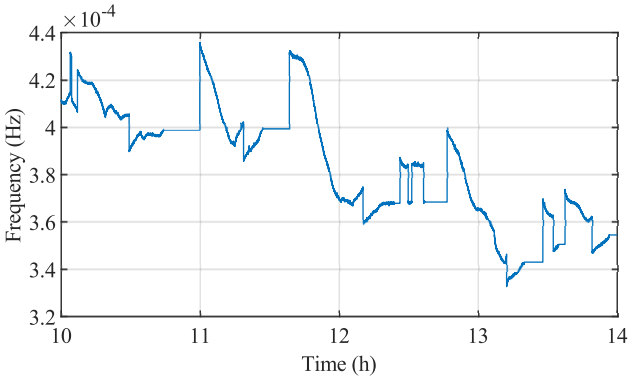

FIGURE 7. Calculated cutoff frequency for the proposed adaptive frequency-based power manager.

Fig. 8 shows the effect of different low pass filter cutoff frequency values on the battery and supercapacitor power, the battery and supercapacitor SOC, and the battery and PV converter. Initially, the cutoff frequency is set at 0.00057 Hz. The cutoff frequency is reduced in the second test and set at 0.0003 Hz. Fig. 8(a), Fig. 8(b), and Fig. 8(c) show the results for a cutoff frequency of 0.00057 Hz, while Fig. 8(d), Fig. 8.(e), and Fig. 8(f) show the results for a cutoff frequency of 0.0003 Hz.

Initially, there is a surplus of generated energy (P_{PV}), and both the battery and supercapacitor are charging as shown in Fig. 8(a) and Fig. 8(d). The filter with a higher cutoff frequency provides a faster growth in the battery power, SOC_{BAT} and I_{Lbat}, as depicted in Fig. 8(b) and Fig. 8(c), compared with the results of the filter with a lower cutoff frequency, shown in 8(e) and Fig. 8(f). Also, the supercapacitor charges slowly for a higher cutoff frequency as the battery assumes a larger charging power. Conversely,

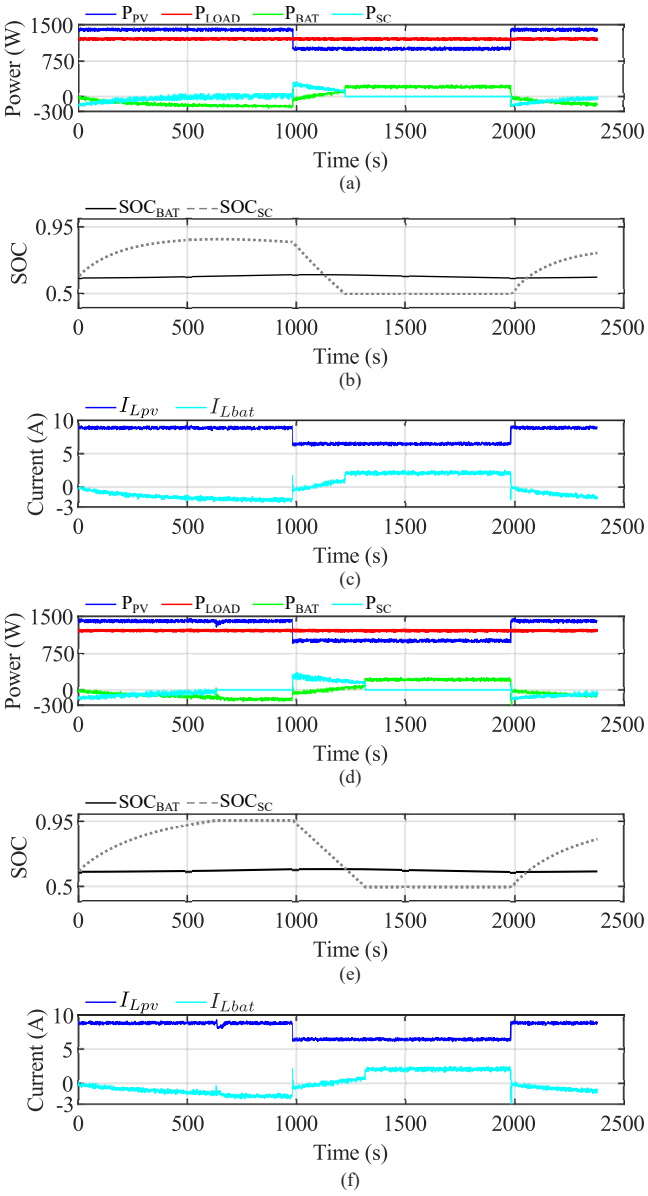

FIGURE 8. Effect of two different low pass filter cutoff frequencies: (a) Powers using $f_c = 0.00057\ Hz$; (b) Battery and supercapacitor SOC using $f_c = 0.00057\ Hz$; (c) Battery and PV converter currents using $f_c = 0.00057\ Hz$; (d) Powers using $f_c = 0.0003\ Hz$; (e) Battery and supercapacitor SOC using $f_c = 0.0003\ Hz$; (f) Battery and PV converter currents using $f_c = 0.0003\ Hz$.

a lower cutoff frequency makes the supercapacitor charge faster, reaching the maximum allowed SOC, as seen in Fig. 8(e). At this moment, the battery is the only active storage element, as shown by the powers depicted in Fig. 8(d). Then, the PV converter operates in the LPPT to avoid abrupt power changes in the battery. The effect of the transition between MPPT and LPPT can be seen by the small transient in the I_{Lpv} current presented in Fig. 8(f).

Just before the time 1000 s, there is a deficit of generated energy. The battery power increases faster for the filter with a higher cutoff frequency, as noticed by comparing Fig. 8(a) and Fig. 8(d). When the power deficit occurs, the SOC of the supercapacitor for the system with a higher cutoff frequency is not maximum. In comparison, the SOC of the supercapacitor for the system with a lower cutoff frequency is maximum. It can be observed in Fig. 8(b) and 8(e). Therefore, the supercapacitor depletes earlier when a higher cutoff frequency is used, and the battery also provides the power deficit earlier when compared with a system with a lower cutoff frequency. Fig. 8(b) and Fig. 8(e) show this behavior.

As shown in Fig. 8, different cutoff frequency values impact the power behavior and, consequently, the battery's current. Small cutoff frequency values lead to smoother battery current and SOC changes, while higher cutoff frequency implies faster current and SOC changes.

V. CONCLUSION

This paper presented a new adaptive frequency-based power management system for HESS. The HESS is composed of a battery and a supercapacitor. The novelty relies on a simple method to define the low-pass filter's cutoff frequency to generate real-time power references for the battery and supercapacitor. The motivation behind this study came from the distinct characteristics of batteries and supercapacitors. Batteries have high energy density but low power density, whereas supercapacitors exhibit low energy density but high power density. This pairing proves advantageous for PV systems, given that irradiance and load undergo fluctuations in their profile. Using these storage components with adequate power management provides consistent power delivery to the load.

The proposed strategy to calculate the cutoff frequency considers the State of Power (SOP) and the State of Energy (SOE) of the battery. It considers the actual point of operation of the battery, which is variable over time. The method provides a smoother current profile for the battery that reduces power dissipation and contributes to improving the battery lifespan.

The proposed adaptive frequency-based strategy for HESS power management was compared with two other strategies: a rule-based approach and the fixed frequency-based method. Compared to these strategies, the results show that the proposed method efficiently reduces the oscillations in the current delivered to the battery. The proposal also reduced the power dissipated in the battery with a similar cycle usage of the rule-based method. Also, the HESS operating with the proposed approach provides better energy efficiency.

ACKNOWLEDGMENT

The present work was carried out with the support of the Coordenação de Aperfeiçoamento de Pessoal de Nível Superior - Brazil (CAPES) - Financing Code 001, CNPq processes 405700/2021-0 and 306633/2022-1, NAPI - Sudoeste, Fundação Araucária and UTFPR - Campus Pato Branco. This research was partly supported by the Estonian

Research Council grant PRG1086 and the Estonian Centre of Excellence in Energy Efficiency, ENER (grant TK230), funded by the Estonian Ministry of Education and Research.

AUTHOR'S CONTRIBUTIONS

GONSCHOROWSKI, E.: Conceptualization, Data Curation, Formal Analysis, Investigation, Methodology, Software, Validation, Visualization, Writing – Original Draft, Writing – Review & Editing. **CARDOSO, R.**: Conceptualization, Formal Analysis, Funding Acquisition, Investigation, Methodology, Project Administration, Resources, Supervision, Validation, Visualization, Writing – Original Draft, Writing – Review & Editing. **CARVALHO, E.L.**: Conceptualization, Formal Analysis, Investigation, Methodology, Software, Writing – Review & Editing. **STEIN, C.M.O**: Formal Analysis, Funding Acquisition, Methodology, Resources, Writing – Review & Editing. **CARATI, E.G.**: Formal Analysis, Funding Acquisition, Methodology, Resources, Writing – Review & Editing. **DENARDIN, G.W.**: Formal Analysis, Funding Acquisition, Methodology, Resources, Writing – Review & Editing. **DA COSTA, J.P.**: Formal Analysis, Funding Acquisition, Methodology, Resources, Writing – Review & Editing.

PLAGIARISM POLICY

This article was submitted to the similarity system provided by Crossref and powered by iThenticate – Similarity Check.

REFERENCES

[1] W. Jing, C. H. Lai, S. H. W. Wong, M. L. D. Wong, "Battery-supercapacitor hybrid energy storage system in standalone dc microgrids: a review", *IET Renewable Power Generation*, vol. 11, pp. 461–469, Mar. 2017, doi:10.1049/iet-rpg.2016.0500.

[2] L. N. Santos, G. G. Sousa, G. A. Salvatti, E. G. Carati, J. P. da Costa, R. Cardoso, C. M. O. Stein, Z. L. I. Nadal, "A Distributed Generation Manager with support for Distributed Network Operator Commands", *in 2020 IEEE International Conference on Industrial Technology (ICIT)*, pp. 810–815, Apr. 2020, doi:10.1109/ICIT45562.2020.9067315.

[3] S. Hajiaghasi, A. Salemnia, M. Hamzeh, "Hybrid energy storage system for microgrids applications: A review", *Journal of Energy Storage*, vol. 21, pp. 543–570, Feb. 2019, doi:https://doi.org/10.1016/j.est.2018.12.017.

[4] T. S. Babu, K. R. Vasudevan, V. K. Ramachandaramurthy, S. B. Sani, S. Chemud, R. M. Lajim, "A Comprehensive Review of Hybrid Energy Storage Systems: Converter Topologies, Control Strategies and Future Prospects", *IEEE Access*, vol. 8, pp. 148702–148721, Aug. 2020, doi:10.1109/ACCESS.2020.3015919.

[5] R. C. de Barros, W. C. S. Amorim, W. d. C. Boaventura, A. F. Cupertino, V. F. Mendes, H. A. Pereira, "Methodology for BESS Design Assisted by Choice Matrix Approach", *Eletrônica de Potência*, vol. 29, p. e202412, Jun. 2024, doi:10.18618/REP.2005.1.019027, URL: https://journal.sobraep.org.br/index.php/rep/article/view/916.

[6] "Hybrid electrochemical energy storage systems: An overview for smart grid and electrified vehicle applications", *Renewable and Sustainable Energy Reviews*, vol. 139, p. 110581, Apr. 2021, doi:https://doi.org/10.1016/j.rser.2020.110581.

[7] "A comparison study of different semi-active hybrid energy storage system topologies for electric vehicles", *Journal of Power Sources*, vol. 274, pp. 400–411, Jan. 2015, doi:https://doi.org/10.1016/j.jpowsour.2014.10.061.

[8] D. Xu, Q. Liu, W. Yan, W. Yang, "Adaptive Terminal Sliding Mode Control for Hybrid Energy Storage Systems of Fuel Cell, Battery and Supercapacitor", *IEEE Access*, vol. 7, pp. 29295–29303, Feb. 2019, doi:10.1109/ACCESS.2019.2897015.

[9] H. Rezaei, S. E. Abdollahi, S. Abdollahi, S. Filizadeh, "Energy management strategies of battery-ultracapacitor hybrid storage systems for electric vehicles: Review, challenges, and future trends", *Journal of Energy Storage*, vol. 53, p. 105045, Sep. 2022, doi:https://doi.org/10.1016/j.est.2022.105045.

[10] E. L. Carvalho, L. V. Bellinaso, R. Cardoso, L. Michels, "Price-Based DC Bus Signaling for Nanogrids Power Management", *in 2021 Brazilian Power Electronics Conference (COBEP)*, pp. 1–5, Jan. 2021, doi:10.1109/COBEP53665.2021.9684069.

[11] E. L. Carvalho, L. V. Bellinaso, R. Cardoso, L. Michels, "Distributed Price-Based Power Management for Multibuses DC Nanogrids EEMS", *IEEE Journal of Emerging and Selected Topics in Power Electronics*, vol. 10, no. 5, pp. 5509–5521, Feb. 2022, doi:10.1109/JESTPE.2022.3152101.

[12] L. V. Bellinaso, E. L. Carvalho, R. Cardoso, L. Michels, "Price-Response Matrices Design Methodology for Electrical Energy Management Systems Based on DC Bus Signalling", *Energies*, vol. 14, no. 6, Mar. 2021, doi:10.3390/en14061787.

[13] F. Naseri, S. Karimi, E. Farjah, E. Schaltz, "Supercapacitor management system: A comprehensive review of modeling, estimation, balancing, and protection techniques", *Renewable and Sustainable Energy Reviews*, vol. 155, p. 111913, Mar. 2022, doi:https://doi.org/10.1016/j.rser.2021.111913.

[14] R. Al Badwawi, W. R. Issa, T. K. Mallick, M. Abusara, "Supervisory Control for Power Management of an Islanded AC Microgrid Using a Frequency Signalling-Based Fuzzy Logic Controller", *IEEE Transactions on Sustainable Energy*, vol. 10, no. 1, pp. 94–104, Apr. 2019, doi:10.1109/TSTE.2018.2825655.

[15] H. Liao, J. Peng, Y. Wu, H. Li, Y. Zhou, X. Zhang, Z. Huang, "Adaptive Split-Frequency Quantitative Power Allocation for Hybrid Energy Storage Systems", *IEEE Transactions on Transportation Electrification*, vol. 7, no. 4, pp. 2306–2317, 2021, doi:10.1109/TTE.2021.3070849.

[16] R. Pan, Y. Wu, Y. Wang, J. Chen, L. Wang, "Adaptive power allocation strategy for hybrid energy storage system based on driving pattern recognition", *Journal of Energy Storage*, vol. 83, p. 110787, Apr. 2024, doi:https://doi.org/10.1016/j.est.2024.110787.

[17] G. A. Salvatti, E. G. Carati, J. P. d. Costa, R. Cardoso, C. M. Stein, "Integration of electric vehicles in smart grids for optimization and support to distributed generation", *in 2018 13th IEEE International Conference on Industry Applications (INDUSCON)*, pp. 963–970, Jan. 2018, doi:10.1109/INDUSCON.2018.8627290.

[18] X. Chen, W. Xie, "Research on Safety Control Method of Power Grid Energy Storage System Based on Neural Network Model", *IEEE Access*, vol. 11, pp. 101339–101346, Sep. 2023, doi:10.1109/ACCESS.2023.3314588.

[19] F. Härtel, T. Bocklisch, "Minimizing Energy Cost in PV Battery Storage Systems Using Reinforcement Learning", *IEEE Access*, vol. 11, pp. 39855–39865, Apr. 2023, doi:10.1109/ACCESS.2023.3267978.

[20] P. Singh, J. S. Lather, "Dynamic power management and control for low voltage DC microgrid with hybrid energy storage system using hybrid bat search algorithm and artificial neural network", *Journal of Energy Storage*, vol. 32, p. 101974, Dec. 2020, doi:https://doi.org/10.1016/j.est.2020.101974.

[21] A. A. Kebede, T. Kalogiannis, J. Van Mierlo, M. Berecibar, "A comprehensive review of stationary energy storage devices for large scale renewable energy sources grid integration", *Renewable and Sustainable Energy Reviews*, vol. 159, p. 112213, May. 2022, doi:https://doi.org/10.1016/j.rser.2022.112213.

[22] L. H. Meneghetti, E. L. Carvalho, E. G. Carati, G. W. Denardin, J. P. da Costa, C. M. de Oliveira Stein, R. Cardoso, "Hybrid Inverter and Control Strategy for Enabling the PV Generation Dispatch Using Extra-Low-Voltage Batteries", *Energies*, vol. 15, no. 20, Oct. 2022, doi:10.3390/en15207539.

[23] E. Gonschorowski, R. Cardoso, E. L. Carvalho, C. M. de Oliveira Stein, E. G. Carati, G. W. Denardin, J. P. da Costa, "Analysis of the Use of Supercapacitors and Batteries as Energy Storage Elements for Off-Grid Hybrid Photovoltaic Inverters", *in 2023 IEEE 8th Southern Power Electronics Conference and 17th Brazilian Power Electronics Conference (SPEC/COBEP)*, pp. 1–7, Feb. 2023, doi:10.1109/SPEC56436.2023.10407182.

[24] H. GUENTRI, T. ALLAOUI, M. MEKKI, M. DENAI, "POWER management and control of A PHOTOVOLTAIC system with hybrid battery-supercapacitor energy storage BASED ON HEURISTICS METHODS", *Journal of Energy Storage*, vol. 39, p. 102578, Jul. 2021, doi:https://doi.org/10.1016/j.est.2021.102578.

[25] J. Snoussi, S. B. Elghali, M. Benbouzid, M. F. Mimouni, "Optimal Sizing of Energy Storage Systems Using Frequency-Separation-Based Energy Management for Fuel Cell Hybrid Electric Vehicles", *IEEE Transactions on Vehicular Technology*, vol. 67, no. 10, pp. 9337–9346, Aug. 2018, doi:10.1109/TVT.2018.2863185.

[26] L. F. Costa, R. P. Torrico-Bascopé, "Stand-alone Photovoltaic System with Three Energy Processing Stages", *Eletrônica de Potência*, vol. 16, no. 4, p. 348–356, Nov. 2011, doi:10.18618/REP.20114.348356, URL: https://journal.sobraep.org.br/index.php/rep/article/view/576.

[27] F. G. Nimitti, A. M. S. S. Andrade, "Análise e Desenvolvimento de um Conversor Bidirecional Não Isolado Baseado no Conversor Boost/ Buck CC-CC", vol. 27, p. 325–334, Oct. 2022, doi:10.18618/REP.2022.4.0006, URL: https://journal.sobraep.org.br/index.php/rep/article/view/141.

[28] H. Jank, W. Alegranci Venturini, G. Guilherme Koch, M. L. da Silva Martins, F. Ecke Bisogno, V. Foletto Montagner, H. Pinheiro, "Controle Baseado Em Um LQR Com Estabilidade Robusta À Incerteza Paramétrica Aplicado A Um Carregador De Baterias", *Eletrônica de Potência*, vol. 22, no. 4, p. 408–417, Dec. 2017, doi:10.18618/REP.2017.4.2713, URL: https://journal.sobraep.org.br/index.php/rep/article/view/248.

[29] D. I. Brandão, F. P. Marafão, F. A. S. Gonçalves, M. G. Villalva, J. R. Gazoli, "Estratégia De Controle Multifuncional Para Sistemas Fotovoltaicos De Geração De Energia Elétrica", *Eletrônica de Potência*, vol. 18, no. 4, p. 1206–1214, Nov. 2013, doi:10.18618/REP.2013.4.12061214, URL: https://journal.sobraep.org.br/index.php/rep/article/view/453.

[30] C. C. C. dos Santos, C. F. Moraes, J. P. da Costa, C. M. O. Stein, E. G. Carati, R. Cardoso, "Photovoltaic Boost Converter Control Operating in the MPPT and LPPT Modes", *in 2019 IEEE 15th Brazilian Power Electronics Conference and 5th IEEE Southern Power Electronics Conference (COBEP/SPEC)*, pp. 1–6, Apr. 2019, doi:10.1109/COBEP/SPEC44138.2019.9065604.

[31] C. C. C. dos Santos, J. P. da Costa, C. M. O. Stein, E. G. Carati, R. Cardoso, Z. L. I. Nadal, "Estratégia de Controle para Conversor Boost Fotovoltaico Operando nos Modos MPPT e LPPT", *Eletrônica de Potência*, vol. 25, no. 3, p. 326–336, Sep. 2020, doi:10.18618/REP.2020.3.0006, URL: https://journal.sobraep.org.br/index.php/rep/article/view/317.

[32] Z. He, Y. Li, Y. Sun, S. Zhao, C. Lin, C. Pan, L. Wang, "State-of-charge estimation of lithium ion batteries based on adaptive iterative extended Kalman filter", *Journal of Energy Storage*, vol. 39, p. 102593, Jul. 2021, doi:https://doi.org/10.1016/j.est.2021.102593.

[33] P. Shrivastava, P. A. Naidu, S. Sharma, B. K. Panigrahi, A. Garg, "Review on technological advancement of lithium-ion battery states estimation methods for electric vehicle applications", *Journal of Energy Storage*, vol. 64, p. 107159, Aug. 2023, doi:https://doi.org/10.1016/j.est.2023.107159.

[34] X. Lai, Y. Huang, X. Han, H. Gu, Y. Zheng, "A novel method for state of energy estimation of lithium-ion batteries using particle filter and extended Kalman filter", *Journal of Energy Storage*, vol. 43, p. 103269, Nov. 2021, doi:https://doi.org/10.1016/j.est.2021.103269.

[35] T. Zhang, N. Guo, X. Sun, J. Fan, N. Yang, J. Song, Y. Zou, "A Systematic Framework for State of Charge, State of Health and State of Power Co-Estimation of Lithium-Ion Battery in Electric Vehicles", *Sustainability*, vol. 13, no. 9, Mar. 2021, doi:10.3390/su13095166.

[36] Canadian Solar, "KuDymond CS3U-P-AG Solar Panel Datasheet", Accessed: 2024-07-23, 2020, URL: https://www.canadiansolar.com/wp-content/uploads/2020/05/Canadian_Solar-Datasheet-KuDymond_CS3U-P-AG_EN.pdf.

[37] Eaton, "XTM-18 Supercapacitor Module Datasheet", Accessed: 2024-07-23, 2020, URL: https://www.mouser.com/datasheet/2/87/eaton_xtm_18_supercapacitor_module_data_sheet-1660551.pdf.

[38] S. S. E. B. Division, *Samsung ICR18650-22F Battery Datasheet*, June 2023, URL: https://www.dnkpower.com/wp-content/uploads/2018/04/Samsung-ICR18650-22F-Datasheet.pdf, accessed: 2024-06-06.

[39] S. Ma, M. Jiang, P. Tao, C. Song, J. Wu, J. Wang, T. Deng, W. Shang, "Temperature effect and thermal impact in lithium-ion batteries: A review", *Progress in Natural Science: Materials International*, vol. 28, no. 6, pp. 653–666, Dec. 2018, doi:https://doi.org/10.1016/j.pnsc.2018.11.002.

BIOGRAPHIES

Ezequiel Gonschorowski received the B.Sc. degree in electrical engineering from the Federal University of Technology – Paraná (UTFPR), Pato Branco, Brazil, in 2022. Currently, he is pursuing the M.Sc. degree in electrical engineering at UTFPR. His research interest relates to managing hybrid inverters to maximize battery lifespan.

Rafael Cardoso received the B.S. degree in electrical engineering from the Federal University of Santa Maria (UFSM), Santa Maria, Brazil, in 2001, the M.Sc. degree in electronic and computer science from the Technological Institute of Aeronautics (ITA), São Paulo, Brazil, in 2003, and the Ph.D. degree in electrical engineering from UFSM, in 2008. Since 2006, he has been with the Federal University of Technology – Paraná (UTFPR), Pato Branco, Brazil, where he is currently a Full Professor. His research interests include automatic control systems, power electronics, power converters control, energy storage systems, smart-grids, and power quality.

Edivan Laercio Carvalho received the B.Sc. and M.Sc. degrees from the Federal University of Technology – Paraná (UTFPR), Pato Branco, Brazil, in 2015, and 2018, respectively, and the Ph.D. degree from Federal University of Santa Maria (UFSM), Santa Maria, Brazil, in 2021, all in electrical engineering. He is currently a Researcher with the Power Electronics Group, Tallinn University of Technology, Tallinn, Estonia. His research interests include high-frequency power converter topologies, netzero energy buildings, and power management systems.

Carlos Marcelo de Oliveira Stein received the B.S., M.S., and Ph.D. degrees in electrical engineering from the Federal University of Santa Maria, Santa Maria, Brazil, in 1996, 1997, and 2003, respectively. Since 2003, he has been with the Federal University of Technology – Paraná (UTFPR), Pato Branco, Brazil, where he is currently a Full Professor. His research interests include high-frequency power converter topologies, distributed generation, power supplies, and soft-switching techniques.

Emerson Giovani Carati received the B. S. degree (1996), the Master degree (1999) and Ph.D. degree (2003) in Electrical Engineering from Federal University of Santa Maria, Brazil. Since 2003, he is with the Federal University of Technology – Paraná (UTFPR), Pato Branco, Brazil, where he is a Full Professor. His research interests are related to control of electrical machines drives, distributed power generation and static converters.

Gustavo Weber Denardin received the B.S., M.Sc., and Ph.D. degrees in electrical engineering from the Federal University of Santa Maria, RS, Brazil, in 2002, 2004, and 2012, respectively. Since 2005, he has been with the Federal University of Technology – Paraná, Pato Branco, Brazil, where he is currently a Full Professor. His research interests include embedded systems, real-time operating systems, instrumentation, communication systems, wireless sensor/actuator networks, and smart-grids.

Jean Patric da Costa received the B.S. degree in electrical engineering, and the master's and Ph.D. degrees from the Federal University of Santa Maria, Santa Maria, Brazil, in 2004, 2006, and 2010, respectively. He is currently a Professor with the Department of Electrical Engineering, Federal University of Technology – Paraná, Pato Branco, Brazil. His research interests include control of static converters, smart grids, ancillary services, and distributed generators.